Elastic modeling-based three-component VSP coordinate reorientation

Timmy Dy, Weiping Gou, Wonkee Kim, Chang-Chun Lee, Priyanka Sadhnani (CGG)*

Summary

Vertical seismic profile (VSP) surveys rely on three-component (3C) geophones to acquire high-resolution data around target reservoirs. These 3C geophones are composed of three independent receivers, mounted orthogonally. When inside the borehole, the orientation of each 3C geophone is unknown. To enhance image stacking power from different receivers, it is necessary to reorient all the 3C VSP receivers to a common coordinate system.

We introduce a VSP coordinate reorientation workflow using elastic finite-difference modeling. The only condition required is an adequate knowledge of the overburden velocity. Since VSPs today are typically acquired to supplement existing surface seismic images, adequate velocity models already exist and this method can almost always be applied effectively. We conduct synthetic tests to demonstrate the robustness of our workflow with a variety of noise levels, velocity errors, and acquisition coverages. We also show a real data example from the deep water Gulf of Mexico (GoM).

Introduction

VSP surveys have long been used to calibrate seismic images to well logs. Today, large 3D VSP surveys are designed for the purpose of acquiring high-resolution seismic images of target reservoirs. VSP surveys rely on three-component geophones to acquire high-resolution data around target reservoirs. These 3C geophones are composed of three independent receivers, mounted orthogonally to each other. The orientation of each 3C receiver is unknown because the VSP tools can rotate during deployment into the borehole before being clamped prior to recording. One of the major challenges of VSP imaging is the reorientation of all the 3C receivers to a common coordinate system in order to enhance stacking power from different receivers. While physical measurements are possible, they are costly and unfeasible. Hence, the burden lies on the data processing to correctly reorient the 3C data based on the recorded data.

Various reorientation methods have been employed over the years using the first arrivals in the data, which are pure compressional (P) waves. The particle motion recorded by the 3C VSP receiver is expected to be in the propagation direction of the incident seismic wave. This direction can be described by a unit vector in a global coordinate system as $\overrightarrow{\boldsymbol{A}} = (A_x, A_y, A_z)$ where A_x, A_y, A_z correspond to the vector component measured along East, North, and vertically upward directions respectively. But because the orientation of the 3C receiver is unknown, an analysis of the direct arrival amplitudes in the recorded data does not yield $\overrightarrow{\boldsymbol{A}}$, but rather $\overrightarrow{\boldsymbol{A'}} = (A'_x, A'_y, A'_z)$ where A'_x, A'_y, A'_z correspond to the normalized amplitudes recorded by the x, y, and z components of the receiver.

The task of reorientation is to determine and apply a 3D rotation matrix $\boldsymbol{R}$, which will reorient the recorded data $\overrightarrow{\boldsymbol{A'}}$ into global coordinates $\overrightarrow{\boldsymbol{A}} = \boldsymbol{R}\overrightarrow{\boldsymbol{A'}}$. In practice, two things must be done: (1) accurately measure $\overrightarrow{\boldsymbol{A'}}$ from the recorded direct arrivals and (2) theoretically predict $\overrightarrow{\boldsymbol{A}}$ by a synthetic propagation direction unit vector $\overrightarrow{\boldsymbol{S}}$ that honors the acquisition geometry of the recorded VSP data. $\boldsymbol{R}$ is then determined by the rotation matrix that minimizes the difference between $\overrightarrow{\boldsymbol{S}}$ and $\boldsymbol{R}\overrightarrow{\boldsymbol{A'}}$. In some form or another, this has been the backbone of nearly all methods of 3C VSP coordinate reorientation for several decades.

Many methods approximate the challenge of full 3D reorientation to a simpler single rotation problem by assuming that the vertical component is known. DiSiena et al. (1981) presented a method for reorienting the horizontal components in a vertical borehole, assuming that the vertical component was known and that the incident P-wave direction stays within the source-receiver plane. His method assumed linear polarization of $\overrightarrow{\boldsymbol{A}}$ and used statistical methods of samples within a direct arrival time window to measure its direction. Zeng and McMechan (2006) introduced two new methods for determining the reorientation of the horizontal components, also assuming that the vertical orientation is known and that $\overrightarrow{\boldsymbol{A}}$ stays within the source-receiver plane. These are reasonable assumptions to make because, generally, one of the components of a 3C VSP points roughly in the direction of the wellbore, albeit with some uncertainty. On the other hand, the assumption that $\overrightarrow{\boldsymbol{A}}$ stays within the source-receiver plane is only valid if the overburden velocity is homogenous and isotropic.

Moving beyond the assumption that $\overrightarrow{\boldsymbol{A}}$ stays within the source-receiver plane requires a way to incorporate velocity information into the estimation of $\overrightarrow{\boldsymbol{A}}$. Gaiser et al. (1982) were the first to estimate $\overrightarrow{\boldsymbol{A}}$ through ray-tracing, but did not use this information to refine their VSP reorientation. Instead, they used it for velocity analysis, which is a promising field of inquiry even today. Greenhalgh and Mason (1995) used ray-tracing to approximate $\overrightarrow{\boldsymbol{A}}$ but attempted to reorient a 3D coordinate system using a single rotation about an axis. Armstrong (2009) used 3D ray-

tracing to approximate $\overrightarrow{\boldsymbol{A}}$, but, again, only attempted to solve a single rotation problem by assuming that the vertical component is exactly aligned with the borehole. Thus far, only Mennano et al. (2013) has successfully presented a fully three-dimensional reorientation method, using 3D-ray tracing to approximate $\overrightarrow{\boldsymbol{A}}$, and applying multiple rotations equivalent to rotating the coordinate axes about Euler angles.

Our paper will present a 3C reorientation workflow based on elastic modeling. Our method achieves a better approximation of the theoretical incident P-wave direction $\overrightarrow{\boldsymbol{A}}$ by generating synthetic data $\overrightarrow{\boldsymbol{S}}$ using 3D elastic finite-difference modeling. For VSP receivers underneath complex salt over burden, which is often the case for subsalt exploration and production in the Gulf of Mexico, this elastic modeling-based method overcomes ray-tracing stability issues. By minimizing an error function, we can then determine the optimal set of Euler angles for full 3D reorientation of the data. We demonstrate the strengths and limitations of this method with synthetic tests and a real data example from the deep water GoM.

Elastic Modeling-Based Reorientation Workflow

The reorientation procedure is done independently for each VSP receiver and consists of three steps:

Step 1: Elastic Modeling to Generate Synthetic Data
We use elastic finite-difference modeling to generate a synthetic data set. Each shot is modeled from its surface location, and the wavefield is recorded as X, Y, and Z components at the VSP location.

Step 2: Measure P-wave direct arrivals for theoretical $\overrightarrow{\boldsymbol{S}}$ (synthetic) and recorded $\overrightarrow{\boldsymbol{A'}}$ (real) data
The P-wave direct arrivals are picked separately on both the synthetic and recorded data sets. The direct arrival is picked on the combined trace by square summation of X, Y, and Z components to increase picking accuracy. A short time window around the direct arrival time is selected. We also discarded shots that had low correlation among the three components within a short time window around the direct arrival. The amplitudes of the synthetic and recorded data are normalized, so that only the directions of the incident P-waves are considered.

Step 3: Scan all possible 3D rotations to minimize the error between theoretical and recorded data
All possible 3D rotation matrices **R**(φ, θ, ψ) are formulated, where φ, θ, ψ are the Euler angles as shown in Figure 1 (Weisstein, 2016).

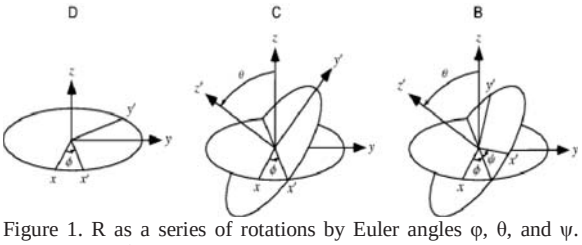

Figure 1. R as a series of rotations by Euler angles φ, θ, and ψ. Image copied from Weisstein (2016).

The goal is to minimize the RMS error function $err(\boldsymbol{R}) = |\overrightarrow{\boldsymbol{A'}} - \boldsymbol{R^{-1}}\overrightarrow{\boldsymbol{S}}|$ by scanning through all possible reorientation angles $\varphi = (0{:}\,2\pi), \theta = (0{:}\,\pi), \psi = (0{:}\,2\pi)$, where $\overrightarrow{\boldsymbol{S}}$ is from the synthetic, $\overrightarrow{\boldsymbol{A'}}$ is from the recorded data, and $\boldsymbol{R^{-1}}$ is the inverse of the rotation matrix $\boldsymbol{R}$.

Theoretically, only a few shots are needed to reorient a receiver, but in practice more than a few shots are necessary to mitigate the uncertainties that come from noise in the real data and errors in the velocity model. Noise can introduce errors in the reorientation angles because it can cause inaccurate measurements of the recorded data $\overrightarrow{\boldsymbol{A'}}$. Inaccurate velocity models, on the other hand, can introduce some errors to the theoretically calculated direction $\overrightarrow{\boldsymbol{S}}$. We designed synthetic tests to demonstrate the effectiveness of the workflow and to test its limitations.

Synthetic Examples

Synthetic data were generated using the final CGG legacy 3D salt model (Figure 2) covering the Jack discovery in Walker Ridge area of the GoM. The density model was originally generated by Zhuo and Ting (2010) for acoustic modeling tests; it was derived from Gardner's equation with additional density perturbations to create sediment reflectors. Elastic finite difference modeling was run to create shot gathers with a maximum frequency of 15 Hz.

Figure 2 also shows the acquisition design of 201 3C VSP receivers distributed vertically with 20 m depth intervals from 6 km to 10 km. Sources were located at the surface on a 100x100 m grid with up to 15 km offsets in both X and Y directions. Synthetic "ideal data" were generated by recording the particle displacements $\overrightarrow{\boldsymbol{A}} = (A_x, A_y, A_z)$ at each receiver location, in the global coordinate system. Random rotations were applied to the each receiver to generate the synthetic "recorded data" $\overrightarrow{\boldsymbol{A'}} = (A'_x, A'_y, A'_z)$ in unknown coordinate orientations, to mimic data from a field acquisition.

We ran the following synthetic tests to assess the robustness of the proposed reorientation workflow. In all tests, we scanned each Euler angle in 1° increments.

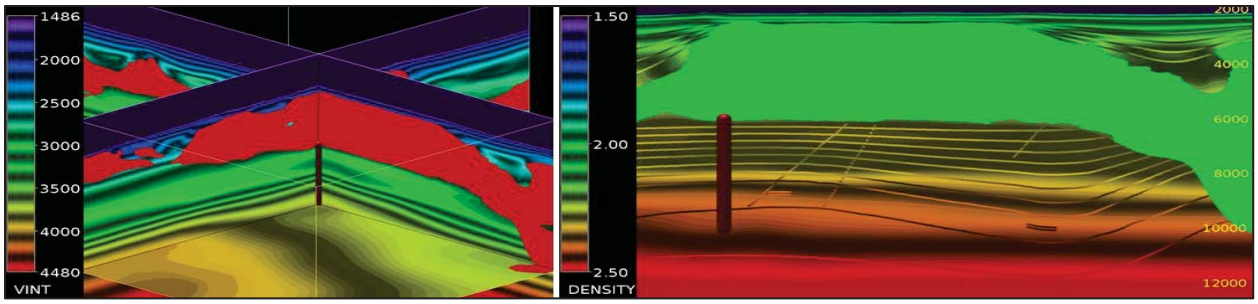

Figure 2. 3D view of Legacy Salt Velocity Model (left) and inline view of Density Model (right), and VSP receiver locations in red.

Test 1: No Noise, Exact Velocity Model

In the ideal case, the theoretically predicted P-wave direction is exactly the "real" P-wave direction ($\vec{S} = \vec{A}$). In this case, our workflow perfectly determined the correct orientations for all 201 receivers. With reorientation applied, energy was more coherent across adjacent VSP receivers (Figure 3).

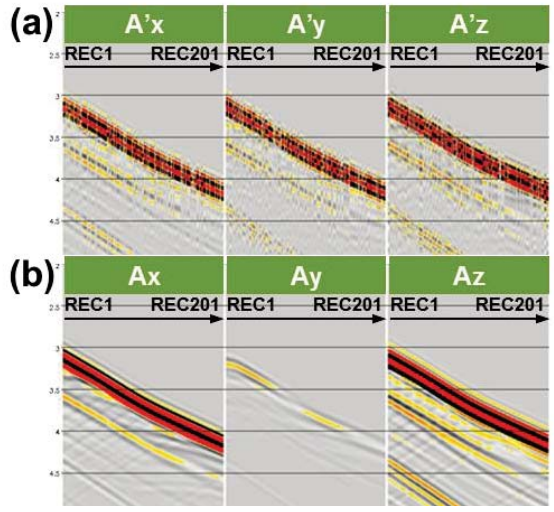

Figure 3. Synthetic Shot Gathers (a) before and (b) after reorientation. Source is 6km East of the VSP location, hence Y-component is very weak after reorientation (to the North).

Test 2: Random Noise, Exact Velocity Model

In the second test, we generated different levels of random noise (Figure 4a) and added it to the recorded data $\overrightarrow{\mathbf{A}'}$ to better simulate real world conditions. The percentage indicated is the maximum amplitude of noise that is added relative to the maximum amplitude of the entire data set. We tested two different types of noise. The first type is coupled noise, where the exact same noise amplitudes are recorded on all three components. The second type is random noise, where different noise is recorded on all three components. We measured the accuracy of the method by plotting histograms of the error in calculated angles when different levels of noise were introduced (Figures 4b and c). The angle error ($\boldsymbol{\delta}$) was calculated for each shot by taking arccosine of the vector dot product between the synthetic and reoriented recorded data: $\boldsymbol{\delta = \cos^{-1}(\vec{S} \cdot \overrightarrow{RA'})}$ This was averaged over all shots for each receiver to produce the angle error for that receiver, contributing one data point to the histogram.

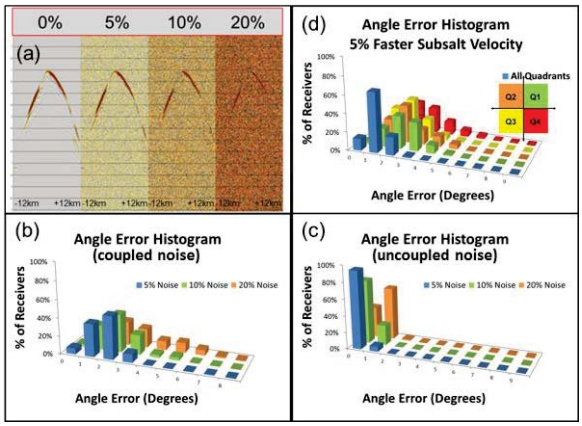

Figure 4. (a) Synthetic data for one shot line recorded by a single receiver at 8km depth showing different levels of added random noise, (b) reorientation angle error histogram with coupled random noise, (c) uncoupled random noise, and (d) no noise, but 5% faster subsalt velocity.

When random noise was coupled across all three components, the majority of receivers had a rotation angle error of less than 3 degrees, and the maximum angle errors were 4°, 6°, and 9° for 5%, 10%, and 20% noise, respectively (Figure 4b). On the other hand, when the noise recorded on the three components was uncoupled, all 201 receivers were correctly reoriented to within 3°, even with as much as 20% added noise (Figure 4c). This difference is explained by the fact that coupled noise is equivalent to noise coming from a specific direction, which slightly biases the orientation. When the random noise is uncoupled, it effectively cancels out any directional bias.

Test 3: No Noise, Inaccurate Velocity Model
For the third test, we increased the subsalt velocity by 5% to see the impact on the reorientation accuracy. The angle error histogram (Figure 4d) shows that all receivers were correctly reoriented to within 4°.

To further evaluate the effects of subsalt velocity errors, we divided the shots into four separate azimuth quadrants and calculated the reorientation angles for each quadrant separately. This time, we were able to see the effects of the velocity error, which increased the angle errors up to 7° (Figure 4d). This was expected from our synthetic model with relatively flat velocity contours, since higher velocities will cause an incident P-wave to come in at a larger angle (measured from the true vertical axis), causing an overcorrection of the z-axis. When data from all quadrants are considered together, the effects cancel each other out.

Real Data Examples

We show the 3C VSP coordinate reorientation results from BP's recent Mad Dog (Green Canyon, GoM) 3D VSP survey, acquired in 2015. Due to the complexity of the velocity overburden and salt geometries, Tilted Transverse Isotropy (TTI) elastic modeling was used for this project.
After 3C reorientation, shot gathers show increased coherency of the data across adjacent receivers, especially for the X and Y components (Figure 5).

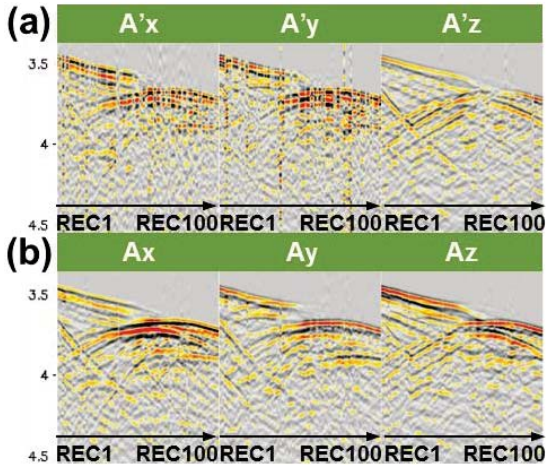

Figure 5. Mad Dog VSP shot gathers (a) before and (b) after VSP coordinate reorientation

Discussion

Based on the synthetic tests, our elastic modeling-based VSP coordinate reorientation workflow works perfectly in ideal conditions. Strong random noise is negligible if it is random across the different components. Strong random noise, when coupled across different components, can introduce angle errors of up to 9°. In field data, noise poses challenges to accurately picking the direct arrival. Stacking energy of the X, Y, and Z components can improve the quality of direct arrival picking. Subsalt velocity errors of 5% can introduce angle errors of up to 3° with full azimuthal shot coverage, and they can introduce small systematic biases of up to 7° when the coverage only contains shots from specific azimuth quadrants. More importantly, the method is shown to work effectively for real data.

Conclusion

As 3D 3C VSP data play increasingly important roles in the development of subsalt reservoirs, accurate reorientation of receiver coordinates can help increase the resolution of the images. A 3D VSP coordinate reorientation workflow using elastic modeling was demonstrated on a synthetic data set and was resilient to random noise and small velocity errors. Real data examples from the Mad Dog field demonstrated an improved coherency among the receivers.

Acknowledgments

We thank BP, BHP Billiton, and Chevron for permission to show the real data example. We also thank CGG for permission to publish this work.

EDITED REFERENCES

Note: This reference list is a copyedited version of the reference list submitted by the author. Reference lists for the 2016 SEG Technical Program Expanded Abstracts have been copyedited so that references provided with the online metadata for each paper will achieve a high degree of linking to cited sources that appear on the Web.

REFERENCES

Armstrong, P., 2009, Model-based relative bearing estimation for a downhole multicomponent sensor array: 79th Annual International Meeting, SEG, Expanded Abstracts, 4100–4104, http://dx.doi.org/10.1190/1.3255727.

DiSiena, J. P., J. E. Gaiser, and D. Corrigan, 1981, Three-component vertical seismic profiles: Orientation of horizontal components for shear wave analysis: 51st Annual International Meeting, SEG, Expanded Abstracts, 1990–2011.

Gaiser, J. E., R. W. Ward, and J. P. DiSiena, 1982, Three-component vertical seismic profiles: Polarization measurements of P-wave particle motion for velocity analysis: 52nd Annual International Meeting, SEG, Expanded Abstracts, 162–165, http://dx.doi.org/10.1190/1.1826869.

Greenhalgh, S. A., and I. M. Mason, 1995, Orientation of a downhole triaxial geophone: Geophysics, **60**, 1234–1237, http://dx.doi.org/10.1190/1.1443852.

Menanno, G., A. Vesnaver and M. Jervis, 2013, Borehole receiver orientation using a 3D velocity model: Geophysical Prospecting, **61**, 215–230.

Weisstein, E. W., 2016, Euler angles: From MathWorld — A Wolfram Web Resource, http://mathworld.wolfram.com/EulerAngles.html, accessed 10 March 2016.

Zeng, X., and G. A. McMechan, 2006, Two methods for determining geophone orientations from VSP data: Geophysics, **71**, no. 4, V87–V97, http://dx.doi.org/10.1190/1.2208935.

Zhuo, L., and C. Ting, 2010, Subsalt steep dip imaging study with 3D acoustic modeling: 80th Annual International Meeting, SEG, Expanded Abstracts, 2956–2960, http://dx.doi.org/10.1190/1.3513460.